JCTC Journal of Chemical Theory and Computation

Article

pubs.acs.org/JCTC

Systematic Expansion of Active Spaces beyond the CASSCF Limit: A GASSCF/SplitGAS Benchmark Study

Konstantinos D. Vogiatzis,[†] Giovanni Li Manni,[†,‡] Samuel J. Stoneburner,[†] Dongxia Ma,[†,‡] and Laura Gagliardi*[,†]

[†]Department of Chemistry, Chemical Theory Center, and Supercomputing Institute, University of Minnesota, Minneapolis, Minnesota 55455-0431, United States

[‡]Max Planck Institut für Festkörperforschung, Heisenbergstraße 1, 70569 Stuttgart, Germany

Supporting Information

ABSTRACT: The applicability and accuracy of the generalized active space self-consistent field, (GASSCF), and (SplitGAS) methods are presented. The GASSCF method enables the exploration of larger active spaces than with the conventional complete active space SCF, (CASSCF), by fragmentation of a large space into subspaces and by controlling the interspace excitations. In the SplitGAS method, the GAS configuration interaction, CI, expansion is further partitioned in two parts: the principal, which includes the most important configuration state functions, and an extended, containing less relevant but not negligible ones. An effective Hamiltonian is then generated, with the extended part acting as a perturbation to the principal space. Excitation energies of ozone, furan, pyrrole, nickel dioxide, and copper tetrachloride dianion are reported. Various partitioning schemes of the GASSCF and SplitGAS CI expansions are considered and compared with the complete active space followed by second-order perturbation theory, (CASPT2), and multireference CI method, (MRCI), or available experimental data. General guidelines for the optimum applicability of these methods are discussed together with their current limitations.

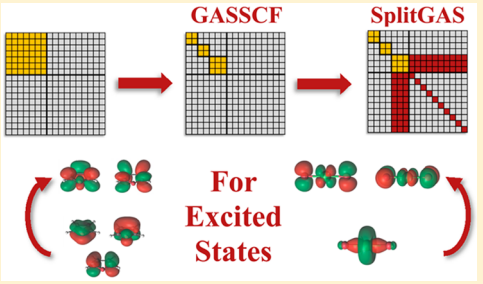

1. INTRODUCTION

The treatment of the correlated motions of electrons constitutes one of the still unsolved challenges of modern electronic structure theory.[1] Correlation energy arises from the erroneous description of the Coulomb repulsion between electrons[2] in the Hartree−Fock theory and can be classified in two types: dynamical correlation and nondynamical or static correlation. Dynamical correlation refers to the instantaneous electron repulsion, and in wave function methods it is usually recovered by electron excitations from the zero-order wave function to the virtual space. Effective approximations from many-body perturbation theory (MBPT)[3] and coupled-cluster theory (CC)[4] provide a quantitative description of dynamical correlation. In density functional theory (DFT), dynamical correlation is instead accounted for by the functional choices. Nondynamical correlation is important for atoms or molecules with nearly degenerate orbitals and with ground or excited states that cannot be described with a single Slater determinant. Typically, such electronic systems are described by a zero-order multiconfigurational wave function, which introduces the nondynamical correlation.[5,6]

One of the most commonly used multiconfigurational methods is the complete active space self-consistent field[7] (CASSCF) method and its extension through second-order perturbation theory[8] (CASPT2). In CASSCF, the configuration space is determined by the electrons and orbitals included in the active space. A full configuration interaction (FCI) wave function is generated within this space, and the orbitals are variationally optimized simultaneously with the configuration coefficients. Redundancies in the orbital rotations are eliminated by accounting only for inactive−active, active−virtual, and inactive−virtual rotations. CASPT2 includes dynamical correlation, and it has been successful in the description of excited states,[9] magnetic properties,[10] and dissociation energies.[11−13] The factorial scaling of the size of the Hilbert space with respect to the size of the active space limits the applicability of CASSCF/CASPT2, which cannot be applied to molecular systems that need active spaces larger than 16 electrons in 16 orbitals.

The exploration of larger active spaces beyond the standard multiconfigurational wave function-based methods is an active field of research. Partitioning of the complete active space (CAS) to smaller subspaces can significantly reduce the number of configuration state functions (CSFs) without affecting the accuracy of the results. Typically, most of the configurations in a configuration interaction (CI) expansion have a minor contribution to the total wave function, i.e., they have a nearly zero coefficient in the configuration expansion. A carefully chosen partition can exclude such configurations and therefore allow the use of larger active spaces. The selection of dominant configurations for a specific state simplifies the wave function

Received: February 26, 2015
Published: May 20, 2015

DOI: 10.1021/acs.jctc.5b00191
J. Chem. Theory Comput. 2015, 11, 3010−3021

without affecting the accuracy of the method. This concept has been successfully used in multireference CI (MRCI) studies.[14−19]

The generalized active space[20,21] (GAS) scheme is an attractive technique for eliminating negligible configurations from the configuration space. In GAS, multiple active spaces are chosen, and interspace excitations are controlled by the user's choice. A suitable choice of the GAS spaces removes the irrelevant configurations from the CI expansion and keeps only configurations with relevant weights. With GASSCF, larger active spaces are accessible than in conventional CASSCF, for example, the GAS5(20,32) for the Gd dimer:[21] 20 electrons in 32 orbitals with five GAS spaces. The occupation restricted multiple active spaces (ORMAS)[22] method relies upon a similar concept. The restricted active space (RAS) scheme used in RASSCF[18,23] and RASPT2[24] is a special case of the GAS scheme, where only three subspaces are chosen, namely, RAS1, RAS2, and RAS3. In the reference space, the RAS1 orbitals are fully occupied, the RAS3 orbitals are empty, and the RAS2 orbitals have occupation ranging from 0 to 2. Restrictions are imposed on the RAS1 and RAS3 excitation level: a predefined maximum number of *holes* in RAS1 and a maximum number of *particles* in RAS3 determine the size of the wave function together with the excitations in the RAS2 space.

A further simplification of the CI expansion is achieved by the SplitCAS[25] method, which is based on partition techniques and targets the recovery of the missing dynamical correlation. In SplitCAS, a CAS CI expansion is partitioned in two subspaces: a principal space (P) and a much larger extended space (Q). Löwdin's partitioning technique[26] approximated to the second order are used to reduce the initial eigenvalue problem to a problem of size equal to the size of the P space. Davidson's reduced model space approach[27,28] and Shavitt's B_k method[29] constitute modifications of this partition technique and share similarities with SplitCAS. Recently, Löwdin's partitioning technique was applied successfully in the spin-flip framework through a quasi-degenerate approximation.[30,31] The more flexible SplitGAS[32] method allows orbital based partitioning of the P and Q spaces, as the GAS scheme is used to select configurations to add in P or in the Q part of the CI expansion. The SplitCAS and SplitGAS approaches capture both static and dynamical correlation, as shown in the case of the Cr_2 dimer.[32]

In this article, a benchmark study of the GASSCF and SplitGAS methods is presented. The effective truncation of an active space to smaller spaces is examined at the GASSCF level. SplitGAS uses this partition concept while, at the same time, capturing the dynamical correlation effects that are missing from GASSCF. These two methods can thus be considered as complementary to each other and are examined together. In the articles in which the methods were first introduced,[21,32] successful calculations of bond dissociation energy curves were reported. In this work, we focus mainly on excited states. A detailed analysis of small, well-documented systems, such as ozone, furan, and pyrrole, allows the exploration of different active space partitions strategies. Analysis of molecules containing a transition metal (copper tetrachloride and linear nickel dioxide) will also be presented.

Our GASSCF results demonstrate the systematic reduction of the CI expansion without loss of accuracy with respect to the equivalent CAS calculations. The exponential scaling in GAS is reduced but not eliminated. Therefore, although GASSCF can be used in combination with larger active spaces compared to that with CASSCF, most dynamic correlation is still not recovered and a quantitative description of excitation energies is out of reach. Conversely, SplitGAS, allowing much larger active spaces, achieves good agreement with available experimental data. For specific cases when experimental data are not available, our results are compared to those obtained at the MRCI level of theory. This article is organized as follows: in Section 2, computational methods are discussed; in Section 3, results for each system are discussed; and, last, Section 4 includes a discussion about the applicability of the methods and suggestions for their further development.

2. COMPUTATIONAL METHODS

All CASSCF, CASPT2, and GASSCF calculations were performed with the MOLCAS-7.8[33] software package. The SplitGAS method is implemented in the LUCIA code[34] and uses one- and two-electron integrals in the molecular orbital (MO) basis obtained from the MOTRA module of MOLCAS-7.8. Internally contracted MRCI[35,36] (icMRCI) calculations were performed with the MOLPRO[37] program package, version 2012.1. In all calculations, scalar relativistic effects were included using a second-order Douglas−Kroll−Hess Hamiltonian. A shifted zeroth-order Hamiltonian was applied to all CASPT2 calculations[38] (IPEA shift) by using the default value of 0.25 au.

The triple-ζ-quality relativistic all-electron ANO-RCC-VTZP[39,40] basis sets were used for ozone, furan, pyrrole, and linear nickel dioxide, contracted to [4s3p2d1f] for oxygen, carbon, and nitrogen, [6s5p3d2f1g] for nickel, and [3s2p1d] for hydrogen. For the copper tetrachloride dianion, the ANO-RCC-VTZP base set was used, contracted to [7s6p5d3f2g1h] for copper and [5s4p2d1f] for chlorine. In the case of nickel dioxide, some basis set dependence was explored by repeating the calculations with the quadruple-ζ-quality ANO-RCC-VQZP basis (contracted to 7s6p4d3f2g for nickel and 5s4p3d2f for oxygen).

The notation CAS(n,m) is followed for the description of the active spaces, where n is the number of electrons and m the number of orbitals. For the GASSCF calculations, a GAS-k(n,m)-n_1e,n_2e,...,n_ie notation is used, where k corresponds to the number of subspaces; n_1, to the maximum number of electrons that can be excited from the first subspace GAS1 to the other subspaces; n_2, to the maximum number of electrons that can be excited from GAS2 to the remaining subspaces, etc.; with $i = k - 1$ (because no electrons can be excited to the last GAS subspace). For example, the notation GAS-3(18,12)-1e,2e means that an active space composed of 18 electrons in 12 orbitals is divided in 3 subspaces, where single electron excitations are allowed from GAS1 to GAS2 and GAS3, and single and double excitations, from GAS2 to GAS3. For the SplitGAS calculations, the SplitGAS-k(n_P,m_P)//(n_T,m_T) notation is used, where k corresponds to the number of subspaces; n_P and m_P are the number of electrons and the number of orbitals in the P space, respectively; T = (P + Q) represents the total molecular space; and n_T and m_T are the number of electrons and the number of orbitals in the T space, respectively.

Two different types of MOs are included in the Q space. The first is doubly occupied valence MOs, which should be correlated for a quantitative calculation of excitation energies. Their choice is system-specific and is based on the chemical nature of the molecule under study, as explained in the next paragraphs. The second (and larger) group of MOs included in

DOI: 10.1021/acs.jctc.5b00191
J. Chem. Theory Comput. 2015, 11, 3010−3021

Table 1. VEEs, IPs and EA of Ozone Obtained at Different Levels of Theory[a]

state	orbitals involved	CASSCF(12,9)	GAS-2(12,9)-1e	CASPT2(12,9)	MRCI	SplitGAS-6 (12,9)//(18,40)	ref
2^1A_1	$(6a_1)^2 \rightarrow (2b_1)^2$, $(4b_2)^2 \rightarrow (2b_1)^2$	4.57	4.54[b]	4.50	4.35[c]	4.59	4.5[f]
1^1A_2	$4b_2 \rightarrow 2b_1$	2.36	2.36	2.02	2.12[c]	2.13	1.6[g] and 1.92[h]
1^1B_1	$6a_1 \rightarrow 2b_1$	2.60	2.59	2.11	2.15[c]	2.24	2.1[h]
1^1B_2	$1a_2 \rightarrow 2b_1$	5.78	5.79	4.91	5.19[c]	5.27	4.86[h,i]
1^3A_2	$4b_2 \rightarrow 2b_1$	2.20	2.19	1.84	1.90[c]	1.75	1.80[h]
1^3B_2	$1a_2 \rightarrow 2b_1$	1.76	1.75	1.75	1.74[c]	1.56	1.43 and 1.29[h]
1^3B_1	$6a_1 \rightarrow 2b_1$	2.24	2.24	1.71	1.73[c]	1.65	1.67[h]
$^2A_1$	e^- lost from $6a_1$	11.49	11.49	12.66	12.44[d]	12.29	12.73[j]
$^2B_2$	e^- lost from $4b_2$	11.42	11.42	12.78	12.49[d]	12.38	13.00[j]
$^2A_2$	e^- lost from $1a_2$	11.97	12.01	13.64	13.17[d]	13.09	13.54[j]
$^2B_2$	e^- added on $2b_1$	3.51	3.53	1.29	1.71[e]	1.52	2.10[k]
MUE		**0.82**	**0.81**	**0.14**	**0.25**	**0.29**	

[a]The mean unsigned error (MUE) compared to the experimental values is reported for all methods. All energies are given in eV. The column ref reports the experimental values. [b]From GAS2(12,9)-2e. [c]Ref 51. [d]Ref 64. [e]Ref 65. [f]Ref 61. [g]Ref 45. [h]Ref 50. [i]Ref 48. [j]Ref 58. [k]Ref 87.

Table 2. VEEs, IPs, and EA of Ozone Calculated from CASSCF(12,9), CASSCF(18,12), and the Corresponding GASSCF at Different Levels of Approximate Active Spaces[a]

state	CAS(12,9)	GAS-2(12,9)-1e	CAS(18,12)	GAS-3(18,12)-1e,1e	GAS-3(18,12)-1e,2e	GAS-3(18,12)-2e,2e
2^1A_1	4.57	4.54[b]	4.42	7.98	4.47	4.45
1^1A_2	2.36	2.36	2.36	2.37	2.42	2.38
1^1B_1	2.60	2.59	2.45	2.48	2.53	2.50
1^1B_2	5.78	5.78	5.68	5.75	5.70	5.68
1^3A_2	2.20	2.19	2.17	2.18	2.23	2.19
1^3B_2	1.76	1.75	1.82	1.74	1.80	1.81
1^3B_1	2.24	2.24	2.06	2.08	2.13	2.07
$^2A_1$	11.49	11.49	11.13	11.26	11.26	11.13
$^2B_2$	11.42	11.42	11.27	11.39	11.38	11.28
$^2A_2$	11.97	12.01	11.85	12.01	11.87	11.84
$^2B_2$	3.51	3.53	3.54	3.55	3.59	3.57
CSFs	666	444	4067	1518	1935	3230

[a]All energies are given in eV. The number of CSFs of the 1^1A_1 ground state is given in the last row. [b]From GAS2(12,9)-2e.

the Q space is composed of virtual orbitals. The selection of the correlated virtual space is based on an orbital energy threshold. The choice of the energy threshold and the truncation of the complete virtual space is discussed in the next paragraphs.

3. RESULTS

3.1. Ozone. This system has been the subject of numerous studies. The availability of both experimental[41−48] and theoretical[49−65] reference values makes it an ideal molecular system for benchmarking the GASSCF and SplitGAS methods. A set of vertical excitation energies (VEEs), ionization potentials (IPs), and an electron affinity (EA) were computed (Table 1) and compared with available experimental data.

Ozone has C_{2v} symmetry at equilibrium. In the calculations, the three O atoms are placed on the *xy* plane. MOs composed of combinations of the 1s (core), 2s, and in-plane $2p_x$ and $2p_y$ atomic orbitals (AOs) belong to either the a_1 or b_2 irreducible representations (irreps) of the C_{2v} point group (Figure S1). The valence 2s, $2p_x$, and $2p_y$ AOs form the σ backbone of the molecule: three bonding σ ($3a_1$, $5a_1$, $4b_2$), three antibonding σ^* ($4a_1$, $5b_2$, $7a_1$), and three nonbonding n_σ ($2b_2$, $6a_1$, $3b_2$) MOs. Combinations of the three out-of-plane $2p_z$ AOs belong to either b_1 or a_2 irreps and form the π system of the molecule. These are the bonding π ($1b_1$), antibonding π^* ($2b_1$), and nonbonding n_π ($1a_2$) orbitals. All valence electrons are correlated in the largest space considered in this study, which is of size (18,54). As shown in Table 1, all VEEs involve one or two electron excitations from the doubly occupied MOs of the ground state to the antibonding π^*. The three IPs involve an electron loss from the nonbonding $3n_\sigma$ ($6a_1$), $4n_\sigma$ ($4b_2$), and n_π ($1a_2$) MOs, respectively. The lowest anionic state, $^2B_2$, used in the calculation of the EA has an extra electron in the antibonding π^* ($2b_1$) MO.

Two CAS choices were considered: CAS(12,9) and CAS(18,12). CAS(12,9) is composed of the nine MOs containing the $2p_x$, $2p_y$, and $2p_z$ AOs. The 1^1A_1 ground state has a multireference character, with the valence electronic structure of the dominant configuration (83%) being $(2\sigma)^2(2n_\sigma)^2(3n_\sigma)^2(4n_\sigma)^2(\pi)^2(n_\pi)^2$ or $(3b_2)^2(5a_1)^2(6a_1)^2(4b_2)^2(1b_1)^2(1a_2)^2$. In CAS(18,12), the 1σ ($3a_1$), $1\sigma^*$ ($4a_1$), and $1n_\sigma$ ($2b_2$) MOs (mostly linear combination of 2s AOs) have also been correlated.

In the GASSCF framework, the (12,9) active space was divided into two subspaces; the first includes the six σ orbitals and the second the three π orbitals. Only single electron excitations were allowed between the two subspaces. This constrained active space is labeled GAS-2(12,9)-1e by following the notation introduced in the previous section. This partition leads to a reduction of the number of CSFs by about 33% compared to those in the corresponding CAS(12,9) calculation. For example, for the 1^1A_1 ground state, 666 CSFs are generated from CAS(12,9), whereas GAS-2(12,9)-1e generates 444. It is

DOI: 10.1021/acs.jctc.5b00191
J. Chem. Theory Comput. 2015, 11, 3010−3021

worth mentioning that with the choice of GAS-2(12,9)-1e the $1^1A_1 \rightarrow 2^1A_1$ excitation cannot be investigated, as it would require a two-electron excitation from GAS1 to GAS2. For this excitation, a GAS2(12,9)-2e scheme has been chosen (see below). Excellent agreement for the VEEs, IPs, and the EA is observed between the parent CAS(12,9) and GAS-2(12,9)-1e calculations, as shown in Table 2.

For the (18,12) active space, the three low-lying 1σ, $1\sigma^*$, and $1n_\sigma$ MOs form the GAS1 active space. As in the GAS-2(12,9)-1e level, the σ-type ($2p_x$, $2p_y$) and π-type MOs belong to different subspaces (GAS2 and GAS3, respectively). Three different interspace excitation schemes have been explored: In GAS3(18,12)-1e,1e, single excitations from GAS1 and from GAS2 are allowed. In GAS-3(18,12)-1e,2e, single excitations out of GAS1 and up to double excitations out of GAS2 are allowed. Finally, in GAS-3(18,12)-2e,2e, up to double excitations out of GAS1 and GAS2 are allowed. The GAS3(18,12)-1e,1e scheme achieves good accuracy in comparison to the parent CAS(18,12) calculation; VEEs, IPs, and EA deviate less than 0.2 eV from CASSCF(18,12), except for the 2^1A_1 state, which involves a two-electron excitation. The GAS-3(18,12)-1e,2e and GAS-3(18,12)-2e,2e further reduce the errors from the parent CAS(18,12). One should notice that these schemes do not fall into the RAS formalism, despite dividing the active space in three subspaces, because the third subspace, GAS3, space contains occupied orbitals.

All VEEs, IPs, and EA values reported in Table 2 show large deviations from the experimental values. The main reason for this disagreement is the lack of correlation energy, which is only partially recovered with the current choice of active space, both at the CASSCF and GASSCF levels. Previous theoretical studies[51,59,62,64,65] have shown that nondynamical correlation alone is not sufficient for a quantitative description of the excitation energies of ozone. In these studies, dynamical correlation is included in the multiconfigurational treatment of the wave function by means of perturbation theory (CASPT2 level),[59] configuration-interaction (MRCI level),[51,64,65] or the EOM-CCSDT formalism.[62] In the present work, dynamical correlation has been added using the SplitGAS method.

In the SplitGAS formalism a combined (P + Q) space of size (18,40) was used. The P space is composed of CAS(12,9), as described above. The extended space in SplitGAS is formed by single excitations out of the 1σ, $1\sigma^*$, and $1n_\sigma$ MOs and single and double excitations into 28 additional canonical virtual orbitals. The choice of only single excitations out of the 1σ, $1\sigma^*$, and $1n_\sigma$ orbitals was motivated by the fact that no significant differences between the GAS-3(18,12)-1e,2e and the GAS-3(18,12)-2e,2e levels were observed at the GASSCF level of theory. In a preliminary investigation (see Supporting Information), various levels of truncation of the virtual orbital space, based on orbital energies, were applied to form the extended (Q) of SplitGAS. Threshold values of 1.0, 2.0, 4.0, and 5.0 E_h (hartree) were considered (Table S1). No significant changes in the VEEs, IPs, and EA were observed for a Q space that included virtual MOs with energies above 2.0 E_h. Conversely, the threshold value of 1.0 E_h was too poor for a quantitative calculation of dynamical correlation. This result lead us to choose 28 virtual orbitals to form the extend space. Table S2 summarizes the number of electrons and orbitals in each subspace. In order to reduce memory requirements, virtual orbitals belonging to different irreps were divided in separate subspaces. In total, six subspaces were considered, SplitGAS-6(12,9)//(18,40). This level of theory includes more than 6 million CSFs in the (P + Q) space for the 1^1A_1 ground state.

The VEEs, IPs, and EA obtained at the SplitGAS-6(12,9)//(18,40) for the 11 states considered are reported in Table 1. For comparison, experimental and computational results from the CASSCF(12,9), GASSCF-2(12,9)-1e, CASPT2(12,9), and MRCI level of theory are also included. The mean unsigned error (MUE) for all theoretical methods in comparison to the experimental values is reported. As previously discussed, CASSCF(12,9) and GASSCF-2(12,9)-1e show similar behavior (the MUE is 0.82 and 0.81 eV, respectively). CASPT2(12,9) captures most of the missing correlation energy and achieves good agreement with the experimental results (MUE = 0.14 eV). MRCI and SplitGAS-6(12,9)//(18,40) have a similar accuracy, with a MUE of 0.25 and 0.29 eV, respectively.

All methods including dynamical correlation considered in this study, i.e., CASPT2, MRCI, and SplitGAS, achieve similar accuracy for the VEEs (on average, deviations were less than 0.2 eV from the reference experimental data). However, the excitation from the ground state to the 1^1B_2 state is a notable exception. The VEE to the 1^1B_2 state calculated with MRCI and SplitGAS deviate from both the experimental reference value of 4.86 eV[48] and the CASPT2(12,9) value of 4.91 eV. Previous theoretical results for this specific state are discussed (Table 3).

Table 3. Comparison among Different Levels of Theory for the VEE from the 1^1A_1 Ground State to the 1^1B_2 Excited State of Ozone[a]

method	1^1B_2 VEE (eV)	no. of CSF
CASPT2[b]	4.69	626
CASPT2 (this work)	4.91	626
EOM-CCSDT[c]	5.13	
MRCI[d]	5.16	10 300
MRCI[e]	5.19	$\sim 39 \times 10^6$
SplitGAS-6(12,9)//(18,40)	5.27	$\sim 6 \times 10^6$
SplitGAS-6(12,9)//(18,42) (LMOs)	5.17	$\sim 8 \times 10^6$
SplitGAS-6(12,9)//(18,54)	5.18	$\sim 25 \times 10^6$
ref[f,g]	4.86	

[a]The number of CSF for the MR methods is also given. [b]Ref 59. [c]Ref 62. [d]Ref 61. [e]Ref 51. [f]Ref 50. [g]Ref 48.

The 1^1B_2 excited state belongs to the Hartley band, which absorbs in the region between 4.2 and 5.6 eV.[46] The Hartley band has the strongest absorption in the spectrum of O_3 below 5.8 eV with an oscillator strength f of about 0.1.[41] A large oscillation strength was calculated at the MRCI level by Elliott et al.[51] for the 1^1B_2 state. The reference value of 4.86 eV used by Musiał et al.[48,62] falls almost in the middle of the absorption region of the Hartley band. CASPT2(12,9) calculations of Borowski et al.[59] underestimated the VEE of 1^1B_2 state by about 0.2 eV (4.69 eV). A better agreement can be achieved by using a shifted zeroth-order Hamiltonian[38] (IPEA shift) in CASPT2 (4.91 eV, this work). Results obtained using equation-of-motion coupled-cluster theory with single, double, and triple excitations (EOM-CCSDT)[62] or MRCI by selecting specific configurations[61] or by using the full configuration space[51] lie between 5.13 and 5.19 eV. SplitGAS-6(12,9)//(18,40), which spans the Q space based on an energy threshold of 2 E_h, predicts the VEE of 1^1B_2 state to be 5.27 eV. This value is slightly higher than the corresponding EOM-CCSDT or MRCI energies. Better agreement can be achieved if a 4 E_h threshold is applied on the Q space, 5.18 eV from the SplitGAS-6(12,9)//

DOI: 10.1021/acs.jctc.5b00191
J. Chem. Theory Comput. 2015, 11, 3010−3021

Table 4. Expansion of Active Spaces for Furan at the CASSCF and GASSCF Level Where Only Excitations from the π-to-π^* Orbitals Are Considered[a]

	CASSCF(6,5)	CASSCF(6,10)	CASSCF(6,15)	CASSCF(6,27)	CASSCF(6,39)
CSFs	28	2510	31 990	1 198 535	11 290 082
1^1B_2	8.09	7.73	7.56	7.51	7.49
2^1A_1	6.85	6.85	6.80	6.79	6.78
3^1A_1	10.25	9.86	9.75	9.70	9.69
1^3A_1	5.47	5.49	5.45	5.44	5.44
1^3B_2	4.02	4.11	4.11	4.12	4.12
		GAS-2(6,10)-1e	GAS-2(6,15)-1e	GAS-2(6,27)-1e	GAS-2(6,39)-1e
CSFs	–	217	406	856	1321
1^1B_2	–	7.78	7.65	7.63	7.64
2^1A_1	–	6.81	6.77	6.77	6.77
3^1A_1	–	9.85	9.77	9.75	9.76
1^3A_1	–	5.45	5.41	5.40	5.40
1^3B_2	–	4.10	4.08	4.07	4.07
		GAS-2(6,10)-2e	GAS-2(6,15)-2e	GAS-2(6,27)-2e	GAS-2(6,39)-2e
CSFs	–	829	2819	12 431	28 913
1^1B_2	–	7.75	7.58	7.53	7.51
2^1A_1	–	6.87	6.80	6.79	6.78
3^1A_1	–	9.88	9.77	9.73	9.71
1^3A_1	–	5.52	5.45	5.44	5.44
1^3B_2	–	4.12	4.11	4.12	4.11

[a]All energies are given in eV. The number of CSFs of the $^1A_1$ ground state is given.

(18,54) level. By localizing the virtual MOs (LMOs) with the Cholesky localization scheme[66] as implemented in MOLCAS, we were able to select MOs with a predominant AO contribution. In the SplitGAS-6(12,9)//(18,42) (LMO) calculation, MOs with 3s3p4s3d contribution were included in the extended Q space. This methodology reduces the VEE of 1^1B_2 state by about 0.1 eV (5.17 eV). The $^3B_2$ state is another state where disagreement between the theoretical methods was found. CASPT2 (1.75 eV) and MRCI (1.74 eV) deviate significantly from the two experimental reference values (1.43 and 1.29 eV), whereas SplitGAS (1.56 eV) and EOM-CCSDT (1.54 eV) are in better agreement.

Finally, IPs calculated at the SplitGAS-6(12,9)//(18,40) level deviate from the experimental reference values[58] by about 0.3 to 0.6 eV and by about 0.1 eV from IPs obtained at the MRCI level by Schmelz et al.[64] CASPT2 results are in better agreement with the reference IPs. A similar behavior is observed for the EA, with the only exception being that CASPT2(12,9) significantly underestimates the experimental value by about 0.8 eV.

3.2. Furan/Pyrrole. The next systems to be discussed are two aromatic five-member molecules: furan and pyrrole. The calibration of our methodology for these two molecules yields information that may be useful for more complicated organic molecules. Furan and pyrrole are isoelectronic and exhibit similar absorption patterns in their UV spectra, i.e., their absorption bands are attributed to the same electronic excitations. Their fully conjugated planar system leads to a weak aromatic 6π-electron character. In C_{2v} symmetry, and for the 1^1A_1 ground state, furan and pyrrole have MOs filled up to $9a_1$, $2b_1$, $1a_2$, and $6b_2$. The occupied π-orbitals are $1b_1$, $2b_1$, and $1a_2$, with the lowest π^* orbitals being $3b_1$ and $2a_2$. The lowest singlet and triplet valence excited states considered in this benchmark study involve π-to-π^* excitations. The VEEs from the ground state to the singlet 2^1A_1, 3^1A_1, and 1^1B_2 and the triplet 1^3A_1 and 1^3B_2 states are examined. Rydberg states are excluded from this study. As discussed by others,[67] the difference in CASPT2 energies from state-specific and state-averaged orbitals is less than 0.1 eV. For simplicity, all results reported in this study are obtained with state-specific CASSCF orbitals. Our results are compared with the experimental data of Flicker et al.[68] Finally, we have recalculated the VEEs of interest with MRCISD(6,5) by using the same CAS(6,5) wave function as that in our SplitGAS calculations.

Table 4 includes VEEs for the first five π-to-π^* excited states of furan calculated with CASSCF and GASSCF. The size of the active spaces has been systematically expanded from (6,5) up to (6,39). The CAS(6,10) includes three b_1 and two a_2 extra virtual MOs. The CAS(6,15) includes five additional virtual MOs (three b_1, two a_2). An increase of the active space results in a decrease of the VEEs of the 1^1B_2 and 3^1A_1 states by about 0.5 eV. Smaller differences are observed for the 2^1A_1, 1^3A_1, and 1^3B_2 states (0.1 eV or less). Energy thresholds of 2.0 and 3.0 E_h, respectively, for the canonical virtual orbitals belonging to b_1 and a_2 irreps lead to the CAS(6,27) and CAS(6,39), respectively. GAS2-type CI expansions have been constructed as follows: the CAS(6,X) space (X = 10, 15, 27, or 39) is divided in two subspaces. The first subspace contains the initial five π-to-π^* orbitals of the minimum CAS(6,5) space, and the second subspace contains the additional virtual orbitals. Single or single and double excitations are allowed from GAS1 to GAS2. These are reported in Table 4 as GAS-2(6,X)-1e and GAS-2(6,X)-2e, respectively. No significant differences are observed for the VEEs when comparing the excitation energies calculated from CASSCF(6,10) and CASSCF(6,15) with the corresponding results from GAS2, although significant reduction of the CI expansion is achieved by the GAS choices. For example, the GAS-2(6,15)-1e and GAS-2(6,15)-2e contain only 1 and 9% of the total number of CSFs, respectively. Increasing the number of unoccupied orbitals (X = 27 or 39) does not affect the VEEs. Among the different approaches presented in Table 4, GAS-2(6,15)-1e is the best choice compared to the parent CAS(6,15) energies, in terms of efficiency and accuracy. The results with a GAS-2(6,15)-1e

DOI: 10.1021/acs.jctc.5b00191
J. Chem. Theory Comput. 2015, 11, 3010−3021

space with additional subspaces, containing doubly occupied and virtual MOs of σ type, are reported in the Supporting Information (Table S3).

Table 5 shows SplitGAS results for the low-lying states of furan and pyrrole. In all cases, the correlated space is divided in six subspaces. The first subspace includes the occupied MOs of the σ system (six a_1 MOs and four b_2 MOs), composed of the 2s, $2p_x$, and $2p_y$ AOs of carbon, oxygen, or nitrogen for furan and pyrrole, respectively. Single and double excitations are allowed from this subspace. The second subspace includes the π system of the aromatic molecules and forms the P space of the SplitGAS calculations. The remaining four spaces are composed of low-lying canonical virtual orbitals, and they form the Q space, chosen according to orbital energy thresholds. The values of 1.0 and 2.0 E_h have been examined, resulting in active spaces (P + Q) with 26 electrons in 55 and 84 orbitals in total, respectively. As can be seen in Table 5, our results considerably deviate from the experimental VEEs for both molecules, with the errors exceeding the 1 eV in some cases. The reason for this divergence is the incorporation of Rydberg-type orbitals inside the Q space, leading to unphysical mixing of Rydberg and valence excited states. Rydberg orbitals could be deleted from the orbital space after separately optimizing the Rydberg excited states.[69,70] In the present work, however, this procedure has been avoided, as our goal is not necessarily the theoretical reproduction of the experimental spectra but, rather, a comparison of SplitGAS and MRCISD (singles and doubles) results by using the same basis set (ANO-RCC-VTZP) and same primary (6,5) space. Reasonable agreement between the two methods is observed for most of the states. For the majority of the excited states, the larger Q space shifts the VEEs closer to the MRCISD values. The biggest deviation was found for the VEE of the 2^1A_1 state. For both aromatic molecules, the VEE to this particular state is not affected by the expansion of the Q space based on an energy threshold.

Table 5. Expansion of Active Spaces for Furan and Pyrrole for SplitGAS[a]

				SplitGAS-6 (6,5)//(26,55)	SplitGAS-6 (6,5)//(26,84)
	state	exp.	MRCI(6,5)	1 hartree	2 hartree
furan	1^1B_2	6.06	6.93	6.94	6.85
	2^1A_1		6.79	7.13	7.13
	3^1A_1	7.82	9.11	9.21	9.10
	1^3A_1	5.22	5.58	5.84	5.79
	1^3B_2	4.05	4.26	4.38	4.33
pyrrole	1^1B_2		7.02	7.15	7.03
	2^1A_1	5.98	6.55	6.92	6.91
	3^1A_1	7.54	8.66	8.78	8.63
	1^3A_1	5.10	5.62	5.85	5.81
	1^3B_2	4.21	4.55	4.71	4.67

[a]Experimental and MRCI VEEs are given for comparison. All energies are given in eV.

3.3. Nickel Dioxide. The nickel atom forms three different conformers with molecular oxygen: a superoxo, a peroxo, and a linear isomer. A recent, detailed MRCI study by Hübner and Himmel[71] showed that the linear ONiO isomer is the lowest energy form of $Ni(O_2)$. This conformation is about 1.53 eV more stable than the cyclic $Ni(O_2)$. Experimental evidence for the existence of the linear ONiO has been found by reaction of laser-ablated Ni atoms with O_2 in argon[72] and neon[73] matrices. The electronic structure of various conformers of the anionic species, $ONiO^-$, has been studied by photoelectron spectroscopy.[74,75] Early theoretical works were focused on the cyclic $Ni(O_2)$ isomer.[76−78] DFT calculations predicted a linear $^1\Sigma_g^+$ ground state[72,79] and placed the peroxo $^3B_1$ state 0.73 eV above the $^1\Sigma_g^+$ state.[72]

The adiabatical excitation energies of the linear ONiO isomer are examined. In particular, the four lowest states, $^1\Sigma_g^+$, $^3\Pi_g$, $^1\Pi_g$, and $^5\Pi_u$, are calculated by symmetrically varying the R_{Ni-O} bond distances. The excitation from the $^1\Sigma_g^+$ ground state to the $^1\Pi_g$ state involves an electron excitation from the $3d_{z^2}$ orbital ($6a_g$) to the π^* orbital ($2b_{3g}$ or $2b_{3g}$). The first triplet state is described by a spin-flip of the electron occupying the π^* orbital of the $^1\Pi_g$ state. The quintet $^5\Pi_u$ state involves two-electron excitations to the π^* orbitals: one-electron excitation from the $3d_{z^2}$ orbital and one-electron from the $2p_x/2p_y$ orbitals.[71] An active space of (18,12) was used in the CASSCF and GASSCF calculations (Figure 1a), which includes the six 4s3d orbitals of nickel and the six 2p orbitals of the two oxygen atoms.

At the GASSCF level, CAS(18,12) is partitioned in three subspaces based on symmetry considerations. The first space (GAS1) is composed of the σ-type MOs, which are the bonding $8a_g$, the antibonding $9a_g$, and the nonbonding $5b_{1u}$ orbitals (Figure 1a). GAS1 also includes the $3d_{z^2}$ and $3d_{xy}$ orbitals belonging to the same irreducible representation as the σ-type (σ and σ^*) MOs. GAS2 includes the π-type MOs, i.e., the two components of the π bonding $1b_{2g}$ and $1b_{3g}$, the π^* antibonding $2b_{2g}$ and $2b_{3g}$, and the nonbonding $3b_{2u}$ and $3b_{3u}$. GAS3 includes only the remaining $3d_{x^2-y^2}$ ($1b_{1g}$) orbital. No excitations from or to GAS3 were allowed. Thus, this partition can be considered equivalent to a CAS(16,11); nonetheless, the (18,12) nomenclature is kept for consistency with subsequent partitioning schemes (*vide infra*). Two different excitation schemes were applied within the three subspaces. The first includes CSFs generated by single electron excitations from GAS1 to GAS2 (GASSCF3(18,12)-1e0e); the second adds two-electron excitations from GAS1 to GAS2 (GASSCF-3(18,12)-2e0e).

The impact of the double-shell of Ni was examined by extending the (18,12) active space to (18,20). The additional 8 virtual MOs are linear combinations of the six 5s4d of Ni and the $3p_x/3p_y$ orbitals of the oxygen atoms. The full (18,20) space is partitioned in 8 subspaces, as shown in Figure 1a. Orbitals $6a_g$, $7a_g$, $8a_g$, $9a_g$, and $5b_{1u}$ form GAS1 (as in the GAS-3(18,12) scheme). The $10a_g$, $11a_g$, and $12a_g$ MOs, which are dominated by contributions from the 5s, $4d_{z^2}$, and $4d_{xy}$ atomic orbitals of Ni, form GAS2. GAS3 is formed by the $1b_{2g}$, $2b_{2g}$, $1b_{3g}$, $2b_{3g}$, $3b_{2u}$, and $3b_{3u}$ orbitals (GAS2 in the GAS-3(18,12) scheme). GAS4 is composed of $4d_{xz}$ and $4d_{yz}$ orbitals ($3b_{2g}$ and $3b_{3g}$, respectively) and the double-shell of the $2p_x/2p_y$ orbitals of the oxygen atoms ($4b_{2g}$ and $4b_{3g}$, respectively). GAS5 contains orbital $1b_{1g}$, whereas $2b_{1g}$ ($4d_{x^2-y^2}$) forms the GAS6 space. The minimum and maximum electron occupations of each subspace are reported in Table S4.

Single and double excitations are allowed from each subspace of the initial CAS(18,12) to the corresponding additional subspaces of the second shell, i.e., from GAS1 to GAS2, from GAS3 to GAS4, and from GAS5 to GAS6. An excitation level between subspaces of different symmetry similar to that in the GAS-3(18,12)-1e0e is followed in this scheme. Only single excitations are allowed between the first two (GAS1 and GAS2) and the next two subspaces (GAS3 and GAS4). No excitations

DOI: 10.1021/acs.jctc.5b00191
J. Chem. Theory Comput. 2015, 11, 3010−3021

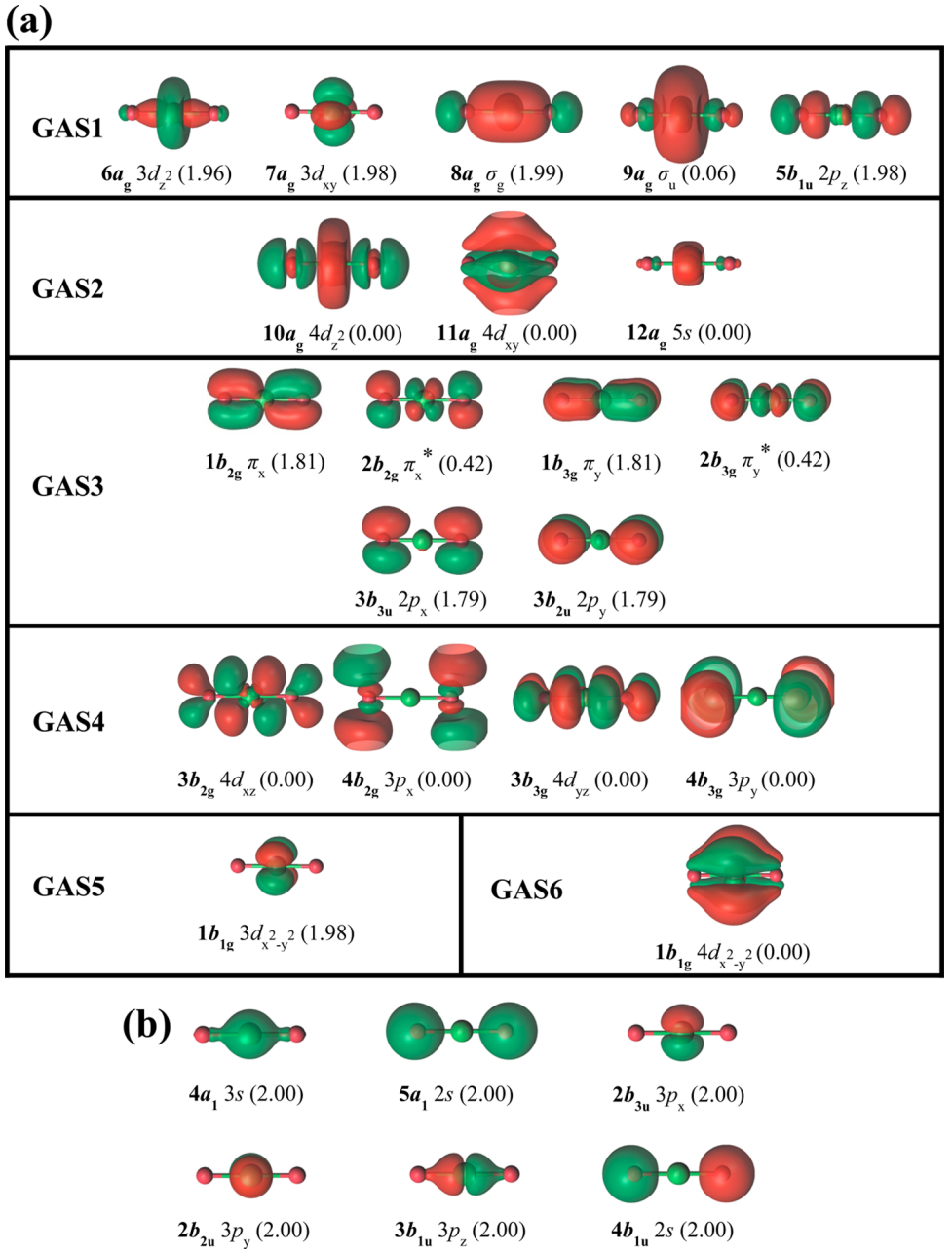

Figure 1. (a) Natural orbitals of linear nickel dioxide at equilibrium bond distance of the $^1\Sigma_g^+$ ground state divided in six subspaces for the GASSCF-6(18,20)-2e1e2e0e2e calculations. GAS1, GAS3, and GAS5 are the same subspaces used for the GAS-3(18,12) scheme. At that level of theory, they are named GAS1, GAS2, and GAS3, respectively. (b) Six orbitals included in the SplitGAS-8(18,12)//(30,35) calculation. Orbital labels and occupation numbers from the parent CAS(18,12) calculation for the $^1\Sigma_g^+$ ground state are listed below each orbital.

are allowed from the first four to the last two subspaces (GAS5 and GAS6). This level of theory is abbreviated as GASSCF-6(18,20)-2e1e2e0e2e and includes about 18 million CSFs. The corresponding CASSCF(18,20) calculation would be prohibitive (more than 1 billion CSFs).

Table 6 reports the adiabatic excitation energies and the R_{Ni-O} bond distances of the minimum of each state ($^1\Sigma_g^+$, $^3\Pi_g$, $^1\Pi_g$, and $^5\Pi_u$). Previous MRCI[71] and DFT[72,73,79−81] results are also included for comparison. The MRCI data were obtained by using CASSCF(18,12) orbitals. It should be noted that in the MRCI reference data, the *semicore* correlation is not included, i.e., the 3s3p orbitals are not correlated, and effects from higher excitations (e.g., second d-shell) are neglected. The authors[71] give a rough estimate of the error introduced from their computational approach of about 0.13 eV, which is essentially from the 3s3p *semicore*−valence correlation. The ANO-RCC basis set, contracted as 7s6p4d3f2g for nickel and 5s4p3d2f for oxygen, was used in the MRCI study. In this study, as already discussed in the Computational Methods section, two different contraction schemes were employed, namely, the same as that in the MRCI study and a smaller one (6s5p3d2f1g for nickel and 4s3p2d1f for oxygen). The basis set effects are discussed at the end of this section.

The wave function constructed by the CASSCF(18,12) level contains 2108 CSFs. Excitation energies obtained at this level are in agreement with MRCI data, whereas the bond distance predicted by CASSCF(18,12) is 0.02 Å longer that the MRCI value. The partition schemes introduced by GASSCF-3(18,12)-

DOI: 10.1021/acs.jctc.5b00191
J. Chem. Theory Comput. 2015, 11, 3010−3021

Table 6. Adiabatic Excitation Energies (in eV) and Ni−O Bond Distances (in Å) for the $^1\Sigma_g^+$, $^3\Pi_g$, $^1\Pi_g$, and $^5\Pi_u$ States of Linear Nickel Dioxide at the Different Levels of Theory Considered in This Study

		$^1\Sigma_g^+$		$^3\Pi_g$		$^1\Pi_g$		$^5\Pi_u$	
method	CSFs of $^1\Sigma_g^+$	E	R_{Ni-O}	E	R_{Ni-O}	E	R_{Ni-O}	E	R_{Ni-O}
GASSCF-3(18,12)-1e0e	709	0	1.63	0.52	1.70	0.84	1.73		
GASSCF-3(18,12)-2e0e	1167	0	1.63	0.58	1.70	0.89	1.73	0.84	1.75
CASSCF(18,12)	2108	0	1.63	0.59	1.70	0.91	1.73	0.89	1.75
GASSCF-6(18,20)-2e1e2e0e2e	18 387 635	0	1.63	0.55	1.68	0.97	1.68	0.81	1.73
CASPT2(18,12)	2108	0	1.61	0.31	1.61	0.69	1.60	1.27	1.68
SplitGAS-8(18,12)//(30,35)	39 763 303	0	1.59	0.33	1.61	0.82	1.61	0.64	1.68
SplitGAS-8(18,12)//(30,35)[a]	39 763 303	0	1.62	0.42	1.65	1.01	1.68	0.63	1.70
SplitGAS-6(18,12)//(18,29)[a,b]	3 407 698	0	1.62	0.49	1.65	1.05	1.68	0.70	1.70
MRCI(18,12)[c]		0	**1.61**	**0.54**	**1.64**	**0.94**	**1.63**	**1.17**	**1.71**
other (DFT studies)			1.586−1.613[d,e,f,g]	0.35[e], 0.41[f]				1.01[f]	

[a]Same basis as MRCI(18,12) (contracted as 7s6p4d3f2g for Ni and 5s4p3d2f for O). [b]No *semicore* correlation. See text for details. [c]Ref 71. [d]Ref 79. [e]Ref 72. [f]Ref 73. [g]Ref 81.

Table 7. Low-Energy Ligand-Field and Charge-Transfer VEEs of $[CuCl_4]^{2-}$ Obtained at Different Levels of Theory[a]

state	CASSCF(11,11)	GASSCF-4(11,11)-0e0eN_{ex}e[c]	CASPT2(11,11)	SplitGAS7(11,11)//(33,37)	exp.[b]
1^2B_{1g}	2.24	2.25	1.52	1.45	1.55
$1^2B_{2g}/1^2B_{3g}$	2.54	2.55	1.77	1.74	1.76
2^2A_g	1.77	1.77	2.00	1.77	
3^2A_g	6.58	6.59	4.60	6.41	
CSFs	26 256	6912		79 307 583	

[a]All energies are given in eV. The number of CSFs of the 1^2A_g ground state is given in the last row. [b]Ref 85. [c]N = 1 for 1^2B_{1g}, 1^2B_{2g}, and 1^2B_{3g} states; N_{ex} = 0 for 2^2A_g, and 3^2A_g states.

1e0e and GASSCF-3(18,12)-2e0e result in adiabatic excitation energies comparable with those of the parent, CASSCF(18,12). The only disagreement is for the $^5\Pi_u$ state for the GAS scheme that allows a single electron excitation between different subspaces (GASSCF-3(18,12)-1e0e). This state involves two-electron excitations to the π^* orbitals, whereas the GASSCF-3(18,12)-1e0e level allows only single excitations. The position of the minimum on the potential energy curves of the four states is not affected by the partition of the CAS(18,12). Using a larger active space (18,20) within the GASSCF framework does not significantly affect the excitation energies. On the other hand, the equilibrium R_{Ni-O} bond distances for the three excited states are in better agreement with the MRCI results.

Dynamical correlation obtained by excitations to the virtual space is introduced by CASPT2 and SplitGAS (Table 6). The CSFs included in the SplitGAS-8(18,12)//(30,35) calculation are constructed by taking into account an active space composed of 30 electrons in 35 orbitals (in P + Q space). The P space is the CAS(18,12) described in the previous paragraph and shown in Figure 1a. *Semicore* MOs of Ni (3s3p) and the two 2s of the oxygen atoms (Figure 1b) and their electrons were used to build the Q space. Seventeen additional low-lying canonical virtual orbitals, which include the double-shell MOs described for the GAS-6(18,20) scheme, are also used to generate configurations in the Q space. Up to two holes were allowed in the MOs formed by the 2s atomic orbitals of the oxygen atoms ($5a_g$, $4b_{1u}$), whereas only single holes were allowed in the 3s3p of Ni. These constraints were based on the fact that the 3s3p MOs of Ni are much lower in energy than the 2s of oxygens. The 17 additional virtual orbitals used for the SplitGAS had mostly 4p5s4d character of Ni and the 3s3p of O. In total, 30 electrons in 35 orbitals were correlated based on the restrictions described above. This partition of the CAS(30,35) generated about 40 million CSFs for the $^1\Sigma_g^+$ ground state and is referred to as SplitGAS-8(18,12)//(30,35).

The SplitGAS-8(18,12)//(30,35) adiabatic excitation energy to the $^3\Pi_g$ state of 0.33 eV agrees with the 0.31 eV energy from CASPT2(18,12) and with previous DFT studies (0.35−0.41 eV), but it is about 0.2 eV lower compared to the MRCI value. The SplitGAS excitation energy to the first singlet $^1\Pi_g$ excited state (0.82 eV) is between the MRCI (0.94 eV) and the CASPT2(18,12) (0.69 eV) values. Finally, the SplitGAS-8(18,12)//(30,35) calculations predict that the quintet $^5\Pi_u$ state is lower than the $^1\Pi_g$ state by about 0.2 eV. On the other hand, both CASPT2(18,12) and MRCI predict the quintet state to lie higher than the $^1\Pi_g$ state and about 1.2 eV higher than the ground state. SplitGAS-8(18,12)//(30,35) and CASPT2(18,12) predict similar equilibrium distances for the $^1\Sigma_g^+$, $^3\Pi_g$, $^1\Pi_g$, and $^5\Pi_u$ states. The R_{Ni-O} distances for these states are shorter than those predicted by the CAS or GAS methods, which lack dynamical correlation.

In ref 71, the ANO-RCC-VQZP (contracted as 7s6p4d3f2g for nickel and 5s4p3d2f for oxygen) was employed. In order to make the comparison more consistent, we have repeated the calculations described above with the same basis set as that in ref 71. These calculations were performed with and without correlating the *semicore* orbitals (SplitGAS-8(18,12)//(30,35) and SplitGAS-6(18,12)//(18,29), respectively). As can be seen in Table 6, SplitGAS and MRCI predict similar excitation energies for the first two excited states. However, the difference between the two methods for the quintet $^5\Pi_u$ state is about 0.5 eV. Finally, the effect on SplitGAS of the *semicore* correlation is estimated to be about 0.07 eV.

3.4. Copper Tetrachloride Dianion. We computed excitation energies to the ligand-field states and to a charge-transfer state of the copper tetrachloride dianion $[CuCl4]^{2-}$. We used the same basis set (ANO-RCC basis set contracted to

DOI: 10.1021/acs.jctc.5b00191
J. Chem. Theory Comput. 2015, 11, 3010−3021

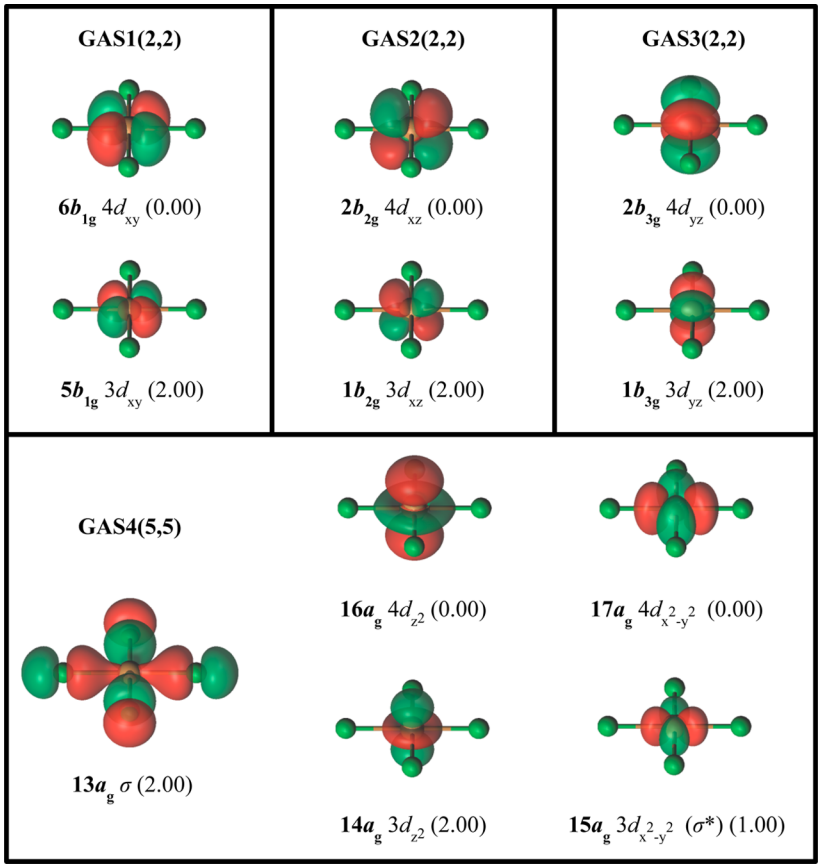

Figure 2. Four subspaces (GAS1(2,2), GAS2(2,2), GAS3(2,2), and GAS4(5,5)) used in the GASSCF-4(11,11) calculations for $[CuCl_4]^{2-}$. Single electron excitations from GAS1, GAS2, or GAS3 to GAS4 are allowed for the 1^2B_{1g}, 1^2B_{2g}, and 1^2B_{3g} excited states, respectively. Orbital labels and occupation numbers for the ^2A_g ground state are listed below each orbital.

[7s6p5d3f2g1h] for Cu and [5s4p2d1f] for Cl) and geometry (planar D_{4h} with R_{Cu-Cl} = 2.291 Å) as those used in previous studies,[82−84] in which the CASPT2(11,11) level of theory was employed.

In the present study, the calculations were performed by imposing D_{2h} symmetry, the highest allowed symmetry in MOLCAS. The orbitals and states are labeled by using the irreps of the D_{2h} point group. The (11,11) active space includes the 3d and 4d orbitals of Cu, and a symmetry-adapted orbital composed of four 3p orbitals of the chlorine atoms pointing toward the metal center. The singly occupied MO has σ^* antibonding character with predominant contribution from the Cu $3d_{x^2-y^2}$ atomic orbital. Excitations from the remaining four 3d orbitals to the σ^* antibonding MO correspond to the 1^2B_{1g}, $1^2B_{2g}/1^2B_{3g}$, and 2^2A_g ligand-field states. A single excitation from the σ Cu−Cl bonding orbital to the σ^* antibonding orbital gives rise to the 3^2A_g charge-transfer state.

Table 7 reports the ligand-field and charge-transfer excitations of $[CuCl_4]^{2-}$ obtained with the different methods discussed in this study. CASPT2(11,11) energies are in good agreement with the experimental values[85] for the first two ligand-field states (1^2B_{1g}, $1^2B_{2g}/1^2B_{3g}$). The GASSCF-4(11,11)-0e0eN_{ex}e partition (N_{ex} = 0 or 1, *vide infra*) is based on symmetry considerations: MOs belonging to the same irrep form a separate subspace (Figure 2). GAS1 includes two b_{1g} orbitals, the $3d_{xy}$, and the isosymmetric $4d_{xy}$ (double-shell). Similarly, GAS2 includes two b_{2g} orbitals ($3d_{xz}$ and $4d_{xz}$) and GAS4 two b_{3g} orbitals ($3d_{yz}$ and $4d_{yz}$). GAS4 includes the five a_g orbitals occupied by 5 electrons in the 1^2A_g ground state. These are the σ bonding (with predominant 3p contribution from the Cl atoms) and σ^* antibonding (predominant contribution from the Cu $3d_{x^2-y^2}$ atomic orbital) character MOs, the $3d_{z^2}$ orbital, and the two corresponding 4d orbitals of Cu (double-shell). Different considerations are accounted for in the calculation of the VEEs. No electron excitations are allowed in the calculations of the 2^2A_g and 3^2A_g states (N_{ex} = 0). The 1^2B_{1g}, 1^2B_{2g}, and 1^2B_{3g} states involve an electron excitation from the 3d orbitals of GAS1, GAS2, or GAS3, respectively, to the $3d_{x^2-y^2}$ orbital ($15a_g$) of GAS4. Thus, single electron excitations (N_{ex} = 1) are allowed from *one* subspace to GAS4 *per state*. For simplicity, this level of theory is referred to as GASSCF-4(11,11)-0e0eN_{ex}e (N_{ex} = 0 or 1). No significant deviations (≥0.01 eV) from those obtained with the parent CASSCF-(11,11) level (Table 7) occur, and the size of the CI expansion is reduced by almost 75%. It should be noted that both CASSCF and GASSCF densities predict a 0.82 ground-state spin population for Cu, whereas the experimental value is 0.62.[86]

Two different P spaces were employed in the SplitGAS calculations. In the first case, the full CAS(11,11) forms the P space. The Q space is composed of single holes created in the 3p orbitals of the four chlorine atoms and double particles in the 15 lowest virtual orbitals, which are split in 5 subspaces. This level of theory is abbreviated SplitGAS-7(11,11)//(33,37) and yields ligand-field excitation energies in agreement with the experiment available values (Table 7). Conversely, no significant contribution to the dynamical correlation for the charge-transfer state (3^2A_g) is observed. The SplitGAS-

DOI: 10.1021/acs.jctc.5b00191
J. Chem. Theory Comput. 2015, 11, 3010−3021

Table 8. Systematic Expansion of the Q Space of SplitGAS for the Low Energy Ligand-Field and Charge-Transfer VEEs of $[CuCl_4]^{2-}$[a]

level		1^2B_{1g}	$1^2B_{2g}/1^2B_{3g}$	3^2A_g	CSFs
	(a) Minimal P- and Q-Spaces				
SplitGAS-4(11,6)//(11,11)		1.06	1.38	8.49	546
	(b) Expansion of *Holes*				
SplitGAS-6(11,6)//(11,41)	no *holes*	1.39	1.64	6.88	12 408
SplitGAS-7(11,6)//(33,52)	1h from 3p Cl	1.30	1.57	6.63	86 079
	2h from 3p Cl	1.25	1.56	6.89	222 630
SplitGAS-7(11,6)//(41,56)	1h from 3s3p Cl	1.31	1.57	6.60	113 171
	2h from 3s3p Cl	1.28	1.59	6.74	369 392
SplitGAS-7(11,6)//(49,60)	1h from 3s3p Cl	1.33	1.59	6.55	140 199
	1h from 3s3p Cu				
	2h from 3s3p Cl	1.29	1.60	6.70	552 936
	2h from 3s3p Cu				
SplitGAS-8(11,6)//(73,72)	2h from 3s3p Cl	1.29	1.60	6.71	1 158 826
	2h from 3s3p Cu				
	1h from 2p Cl				
	(c) Expansion of *Virtual Space*				
SplitGAS-7(11,6)//(49,60)	Threshold: 1.0 E_h	1.33	1.59	6.55	140 199
SplitGAS-7(11,6)//(49,74)	1.5 E_h	1.33	1.67	6.40	1 086 697
SplitGAS-7(11,6)//(49,94)	2.0 E_h	1.34	1.65	6.41	1 848 705
SplitGAS-7(11,6)//(49,122)	2.5 E_h	1.27	1.58	6.50	4 237 455
SplitGAS-7(11,6)//(49,148)	4.0 E_h	1.36	1.97	6.00	6 816 011
SplitGAS-7(11,6)//(49,168)	10.0 E_h	1.50	1.85	5.50	9 215 204
SplitGAS-7(11,6)//(49,206)	all virtual MOs	1.57	1.94	5.10	14 757 732
exp.		1.55	1.76		

[a]All energies in eV. The number of CSFs of the 1^2A_g ground state is given in the last column.

7(11,11)//(33,37) excitation energy for this state is similar to the one obtained at the CASSCF(11,11) level of theory, whereas the CASPT2(11,11) value is about 2 eV lower (see the discussion in the next section). No experimental value is available.

The number of CSFs for the 1^2A_g ground state generated from the SplitGAS-7(11,11)//(33,37) is about 80 million. Thus, this choice of fragmentation of the (33,37) orbital space yields a very large number of CSFs, which does not allow us the flexibility needed for a detailed and systematic exploration of the limits of SplitGAS. For example, the addition of only 9 extra virtual MOs increases the size of the CI expansion to almost 200 million CSFs. Therefore, the CAS(11,11) as P space is not further considered.

A different partition of the active space allowed a significant simplification of the CI problem and the exploration of larger spaces. CAS(11,11) is divided in two subspaces: the σ/σ^* MOs and the four 3d orbitals of Cu form the P space of size (11,6), whereas the second d-shell of Cu is shifted into Q space. The shift of the second d-shell from P space to Q space enables the systematic expansion of the Q space size. However, this choice yielded two problems. First, the CI optimization of SplitGAS reached no convergence for the 2^2A_g state. Second, the initial six MOs included in the P space differ for the 1^2B_{1g}, 1^2B_{2g}, and 1^2B_{3g} states from the MOs of the 1^2A_g ground state; the optimized MOs of CASSCF(11,6), the preceding step of the SplitGAS method, were not the same for the ground and the three excited states. This unbalanced treatment of the P space lead to erroneous VEEs. This issue was overcome by using the MOs of the 1^2A_g ground state as P space for the SplitGAS calculations of the 1^2B_{1g}, 1^2B_{2g}, and 1^2B_{3g} states.

Table 8 report the results obtained by systematically increasing the CI expansion of the ground and excited states of $[CuCl_4]^{2-}$. This is achieved by including more orbitals in the Q space. These orbitals can be either doubly occupied valence orbitals or empty virtual orbitals. In the first case (Table 8b), the number of allowed excitations (*holes*) from these MOs to the (11,6) P space and to the virtual Q space is examined. A calculation with a minimal (11,11) P + Q space, SplitGAS-4(11,6)//(11,11), is the starting point of the systematic expansion of the Q space, and it is reported for completeness (Table 8a). This level of theory fails to provide quantitative results for the excitation energies under study. Table 8b shows the systematic increase of the valence orbitals in which one or two holes are created. For the first two ligand-field states (1^2B_{1g} and $1^2B_{2g}/1^2B_{3g}$), the excitation energies vary between 1.25 and 1.33 eV, and 1.56 and 1.64 eV, respectively. These energies are independent of the number of correlating orbitals and the number of excitations (one or two holes). The excitation energy obtained for the 3^2A_g charge-transfer state differs by about 2 eV from the CASPT2(11,11) value. In Table 8c, the VEEs upon expansion of the virtual space included in the Q space are reported. The choice of the MOs included in the Q space was based on energy considerations. As in the case where the number of holes was systematically increased, the two ligand-field excitations are in agreement with the reference values. For the 1^2B_{1g} state, the difference from the reference value is 0.02 eV, and for the $1^2B_{2g}/1^2B_{3g}$ state, the difference is 0.18 eV. The latter deviation is likely due to the initial choice of P space. The SplitGAS-7(11,11)//(33,37) level is significantly more accurate, where the five 4d orbitals of Cu are included in the P space. Conversely, the VEE of the charge-transfer state is systematically decreased from 6.55 eV (SplitGAS-7(11,6)//(49,60)) to 5.10 eV (SplitGAS-7(11,6)//(49,206)), approaching the value of CASPT2 (4.60 eV). Despite this fortuitous decrease of the 3^2A_g VEE, we conclude that the current

DOI: 10.1021/acs.jctc.5b00191
J. Chem. Theory Comput. 2015, 11, 3010−3021

implementation of the method cannot accurately calculate charge-transfer states when a small Q space is chosen. Suggestions as to how this problem can be overcome are provided in the next section.

4. DISCUSSION AND CONCLUSIONS

The GASSCF method has several interesting features. It can be used to explore large active spaces, which would not be affordable in CASSCF, to detect the contribution of specific excitations (e.g., π to σ^* or π^* orbitals). Moreover, it allows the use of more compact CI expansions than those in the corresponding CASSCF calculations. A systematic extension of the size of the GAS spaces or the number of excitations between GAS spaces results in the capture of a larger portion of static correlation energy. In order to include dynamical correlation, one should include *n*-electron excitations to the virtual MO space. Two bottlenecks hinder the applicability of the method: the exponential scaling of the CI space, since this is a conventional multireference CI expansion, and the lack of a complete incorporation of dynamical correlation. SplitGAS addresses the latter issue by generating larger and more accurate multiconfigurational wave functions. The applicability of the method for the calculation of excited states was demonstrated in this study.

Ozone was the first test case examined. SplitGAS-6(12,9)//(18,40) showed a very good performance for vertical excitation energies with deviations from experimental values not larger than 0.2 eV. The only exception was for the 1^1B_2 state, which was discussed more thoroughly by comparing data from methods that account for both static and dynamical correlation. For ionization energies and electron affinities, SplitGAS performs similarly to MRCI singles and doubles (SD). The π-to-π^* excitations of furan and pyrrole and the four lowest states of nickel dioxide were investigated. For all of these systems, the accuracy of SplitGAS is comparable with that of MRCISD. In both computational methods, the same primary space was used, while the formation of the CI expansion of the extended space differs. Finally, the ligand-field excitations and a charge-transfer state of $[CuCl_4]^{2-}$ were examined by means of the SplitGAS method.

For the case of $[CuCl_4]^{2-}$, when a limited primary space (11,6) was used, the results are affected by unbalanced active spaces for specific excited states. In other words, the MOs included in the P space were not the same for all states. This lead to erroneous results and treatment of ground and excited states on different footing. We overcome this problem by always starting the SplitGAS calcultions from the MOs of the ground state. An alternative approach is the localization of the virtual space, which allows the choice of MOs with favorable predominant character (e.g., the second 4d shell for a 3d-transition metal). This study shows that this approach does not significantly increase the accuracy of the method. Thus, for a more robust treatment of the correlated P and Q spaces, the implementation of an orbital optimization algorithm is necessary, and we are currently working on it. In a SplitGAS-MCSCF-type methodology, the electronic energy is minimized with respect to both the CI expansion and the orbital coefficients.

SplitGAS, like all methods based on perturbation theory, is nonvariational. Therefore, increasing the size of the Q space may affect different states in different ways. As a consequence, energy differences are not necessarily reproduced more accurately by expanding the Q space. This is particularly true when the choice of the size of the Q space is based on an arbitrary energy threshold and not on a choice of physically relevant virtual MOs (e.g., ligand virtual MOs, Rydberg orbitals, etc.). In the $[CuCl_4]^{2-}$ case, for example, a systematic extension of the Q space does not guarantee a systematic increase (or decrease) of the excitation energy (Table 8). On the contrary, fluctuations were observed. We believe that a more systematic choice of orbitals included in the Q space can provide a robust solution that alleviates this discrepancy. This choice should be based on the type of molecular orbitals (determined by their atomic orbital contribution) desired in the extended space. For a diatomic molecule, the atomic orbitals included in Q space can be carefully chosen based on symmetry considerations. This has been effectively demonstrated by the calculation of the dissociation energy curve of the chromium dimer at the SplitGAS-6(12,12)//(24,48) level.[32] For polyatomic systems, like the $[CuCl_4]^{2-}$ molecule, an efficient orbital optimization procedure should be included, similar to that in the CASSCF method. We are making progress in this direction. In such a way, a more physically motivated choice of the orbitals will make the SplitGAS method considerably more accurate.

■ ASSOCIATED CONTENT

Supporting Information

Natural orbitals of the O_3 and furan molecules; SplitGAS and GASSC results for various systems with different active spaces; input example for GASSCF calculations; and equilibrium geometries and point groups. The Supporting Information is available free of charge on the ACS Publications website at DOI: 10.1021/acs.jctc.5b00191.

■ AUTHOR INFORMATION

Corresponding Author

*E-mail: gagliard@umn.edu.

Funding

This work was supported in part by the (U.S.) Department of Energy (DOE), Office of Basic Energy Sciences, under SciDAC grant no. DE-SC0008666.

Notes

The authors declare no competing financial interest.

■ REFERENCES

(1) Tew, D. P.; Klopper, W.; Helgaker, T. *J. Comput. Chem.* **2007**, *28*, 1307.
(2) Löwdin, P.-O. *Phys. Rev.* **1955**, *97*, 1509.
(3) Cremer, D. *Wiley Interdiscip. Rev.: Comput. Mol. Sci.* **2011**, *1*, 509.
(4) Bartlett, R. J.; Musiał, M. *Rev. Mod. Phys.* **2007**, *79*, 291.
(5) Roos, B. O. *Adv. Chem. Phys.* **2007**, *69*, 399.
(6) Szalay, P. G.; Müller, T.; Gidofalvi, G.; Lischka, H.; Shepard, R. *Chem. Rev.* **2012**, *112*, 108.
(7) Roos, B. O.; Taylor, P. R.; Siegbahn, P. E. M. *Chem. Phys.* **1980**, *48*, 157.
(8) Andersson, K.; Malmqvist, P.-Å.; Roos, B. O. *J. Chem. Phys.* **1992**, *96*, 1218.
(9) González, P. D. L.; Escudero, D.; Serrano-Andrés, L. *ChemPhysChem* **2012**, *13*, 28.
(10) Malrieu, J. P.; Caballol, R.; Calzado, C. J.; Graaf, C. d.; Guihéry, N. *Chem. Rev.* **2014**, *114*, 429.
(11) Ruipérez, F.; Aquilante, F.; Ugalde, J. M.; Infante, I. *J. Chem. Theory Comput.* **2011**, *7*, 1640.
(12) Hicks, J.; Hoyer, C. E.; Moubaraki, B.; Li Manni, G.; Carter, E.; Murphy, D. M.; Murray, K. S.; Gagliardi, L.; Jones, C. *J. Am. Chem. Soc.* **2014**, *136*, 5283.

DOI: 10.1021/acs.jctc.5b00191
J. Chem. Theory Comput. 2015, 11, 3010−3021

(13) Brogden, D. W.; Turov, Y.; Nippe, M.; Li Manni, G.; Hillard, E. A.; Clerac, R.; Gagliardi, L.; Berry, J. F. *Inorg. Chem.* **2014**, *53*, 4777.
(14) Buenker, R. J.; Peyerimhoff, S. D.; Butscher, W. *Mol. Phys.* **1977**, *35*, 771.
(15) Huron, B.; Malrieu, J. P.; Rancurel, P. *J. Chem. Phys.* **1973**, *58*, 5745.
(16) Cave, R. J.; Xantheas, S. S.; Feller, D. *Theor. Chim. Acta* **1992**, *83*, 31.
(17) Hanrath, M.; Engels, B. *Chem. Phys.* **1997**, *225*, 197.
(18) Olsen, J.; Roos, B. O.; Jørgensen, P.; Jensen, H. J. A. *J. Chem. Phys.* **1988**, *89*, 2185.
(19) Rolik, Z.; Szabados, Á.; Surján, P. R. *J. Chem. Phys.* **2008**, *128*, 144101.
(20) Fleig, T.; Olsen, J.; Visscher, L. *J. Chem. Phys.* **2003**, *119*, 2963.
(21) Ma, D.; Li Manni, G.; Gagliardi, L. *J. Chem. Phys.* **2011**, *135*, 044128.
(22) Ivanic, J. *J. Chem. Phys.* **2003**, *119*, 9364.
(23) Malmqvist, P. Å..; Rendell, A.; Roos, B. O. *J. Phys. Chem.* **1990**, *94*, 5477.
(24) Malmqvist, P. Å.; Pierloot, K.; Shahi, A. R. M.; Cramer, C. J.; Gagliardi, L. *J. Chem. Phys.* **2008**, *128*, 204109.
(25) Li Manni, G.; Aquilante, F.; Gagliardi, L. *J. Chem. Phys.* **2011**, *134*, 034114.
(26) Löwdin, P.-O. *J. Chem. Phys.* **1951**, *19*, 1396.
(27) Nitzsche, L. E.; Davidson, E. R. *J. Chem. Phys.* **1978**, *68*, 3103.
(28) Staroverov, V. N.; Davidson, E. R. *Chem. Phys. Lett.* **1998**, *296*, 435.
(29) Shavitt, I. *Chem. Phys. Lett.* **1992**, *192*, 135.
(30) Mayhall, N. J.; Goldey, M.; Head-Gordon, M. *J. Chem. Theory Comput.* **2014**, *10*, 589.
(31) Mayhall, N. J.; Head-Gordon, M. *J. Chem. Phys.* **2014**, *141*, 134111.
(32) Li Manni, G.; Ma, D.; Aquilante, F.; Olsen, J.; Gagliardi, L. *J. Chem. Theory Comput.* **2013**, *9*, 3375.
(33) Aquilante, F.; Vico, L. D.; Ferré, N.; Ghigo, G.; Malmqvist, P.-Å.; Neogrády, P.; Pedersen, T. B.; Pitoňák, M.; Reiher, M.; Roos, B. O.; Serrano-Andrés, L.; Urban, M.; Veryazov, V.; Lindh, R. *J. Comput. Chem.* **2010**, *31*, 224.
(34) Olsen, J.; Jørgensen, P.; Simons, J. *Chem. Phys. Lett.* **1990**, *169*, 463.
(35) Werner, H.-J.; Knowles, P. J. *J. Chem. Phys.* **1988**, *89*, 5803.
(36) Knowles, P. J.; Werner, H.-J. *Chem. Phys. Lett.* **1988**, *145*, 514.
(37) Werner, H.-J.; Knowles, P. J.; Knizia, G.; Manby, F. R.; Schütz, M. A. *Wiley Interdiscip. Rev.: Comput. Mol. Sci.* **2012**, *2*, 242.
(38) Ghigo, G.; Roos, B. O.; Malmqvist, P.-Å. *Chem. Phys. Lett.* **2004**, *396*, 142.
(39) Roos, B. O.; Lindh, R.; Malmqvist, P.-Å.; Veryazov, V.; Widmark, P.-O. *J. Phys. Chem. A* **2004**, *108*, 2851.
(40) Roos, B. O.; Lindh, R.; Malmqvist, P.-Å.; Veryazov, V.; Widmark, P.-O. *J. Phys. Chem. A* **2005**, *109*, 6575.
(41) Brand, J. C. D.; Cross, K. J.; Hoy, A. R. *Can. J. Phys.* **1978**, *56*, 327.
(42) Swanson, N.; Celotta, R. J. *Phys. Rev. Lett.* **1975**, *35*, 783.
(43) von Rosenberg, C. W., Jr.; Trainor, D. W. *J. Chem. Phys.* **1975**, *63*, 5348.
(44) McGrath, W. D.; Maguire, J. M.; Thompson, A.; Trocha-Grimshaw, J. *Chem. Phys. Lett.* **1983**, *102*, 59.
(45) Anderson, S. M.; Morton, J.; Mauersberger, K. *J. Chem. Phys.* **1990**, *93*, 3826.
(46) Arnold, D. W.; Xu, C.; Kim, E. H.; Neumark, D. M. *J. Chem. Phys.* **1994**, *101*, 912.
(47) Günther, J.; Anderson, S. M.; Hilpert, G.; Mauersberger, K. *J. Chem. Phys.* **1998**, *108*, 5449.
(48) Steinfeld, J. I.; Adler-Golden, S. M.; Gallagher, J. W. *J. Phys. Chem. Ref. Data* **1987**, *16*, 911.
(49) Thunemann, K.-H.; Peyerimhoff, S. D.; Buenker, R. J. *J. Mol. Spectrosc.* **1978**, *70*, 432.
(50) Palmer, M. H.; Nelson, A. D. *Mol. Phys.* **2002**, *100*, 3601.
(51) Elliott, R.; Compton, R.; Levis, R.; Matsika, S. *J. Phys. Chem. A* **2005**, *109*, 11304.
(52) Zhao, Y.; Tishchenko, O.; Gour, J. R.; Li, W.; Lutz, J. J.; Piecuch, P.; Truhlar, D. G. *J. Phys. Chem. A* **2009**, *113*, 5786.
(53) Bag, A.; Manohar, P. U.; Vaval, N.; Pal, S. *J. Chem. Phys.* **2009**, *131*, 024102.
(54) Barysz, M.; Rittby, M.; Bartlett, R. J. *Chem. Phys. Lett.* **1992**, *193*, 373.
(55) Vaval, N.; Pal, S. *J. Chem. Phys.* **1999**, *111*, 4051.
(56) Kowalski, K.; Piecuch, P. *J. Chem. Phys.* **2004**, *120*, 1715.
(57) Tsuneda, T.; Nakano, H.; Hirao, K. *J. Chem. Phys.* **1995**, *103*, 6520.
(58) Decleva, P.; Alti, G. D.; Lisini, A. *J. Chem. Phys.* **1988**, *89*, 367.
(59) Borowski, P.; Fülscher, M.; Malmqvist, P.-Å.; Roos, B. O. *Chem. Phys. Lett.* **1995**, *237*, 195.
(60) Szalay, P. G.; Bartlett, R. J. *J. Chem. Phys.* **1994**, *101*, 4936.
(61) Banichevich, A.; Peyerimhoff, S. D. *Chem. Phys.* **1993**, *174*, 93.
(62) Musiał, M.; Kucharski, S. A.; Zerzucha, P.; Kuś, T.; Bartlett, R. J. *J. Chem. Phys.* **2009**, *131*, 194104.
(63) Miliordos, E.; Xantheas, S. S. *J. Am. Chem. Soc.* **2014**, *136*, 2808.
(64) Schmelz, T.; Chambaud, G.; Rosmus, P.; Köppel, H.; Cederbaum, L.; Werner, H.-J. *Chem. Phys. Lett.* **1991**, *183*, 209.
(65) Koch, W.; Frenking, G.; Steffen, G.; Reinen, D.; Jansen, M.; Assenmacher, W. *J. Chem. Phys.* **1993**, *99*, 1271.
(66) Aquilante, F.; Pedersen, T. B.; Merás, A. S. d.; Koch, H. *J. Chem. Phys.* **2006**, *125*, 174101.
(67) Serrano-Andres, L.; Merchan, M.; Nebot-Gil, I.; Roos, B. O.; Fulscher, M. *J. Am. Chem. Soc.* **1993**, *115*, 6184.
(68) Flicker, W. M.; Mosher, O. A.; Kuppermann, A. *J. Chem. Phys.* **1976**, *64*, 1315.
(69) Fuelscher, M. P.; Roos, B. O. *J. Am. Chem. Soc.* **1995**, *117*, 2089.
(70) Serrano-Andrés, L.; Roos, B. O. *J. Am. Chem. Soc.* **1996**, *118*, 185.
(71) Hübner, O.; Himmel, H.-J. *J. Phys. Chem. A* **2012**, *116*, 9181.
(72) Citra, A.; Chertihin, G. V.; Andrews, L.; Neurock, M. *J. Phys. Chem. A* **1997**, *101*, 3109.
(73) Allouti, F.; Manceron, L.; Alikhani, M. E. *Phys. Chem. Chem. Phys.* **2006**, *8*, 448.
(74) Wu, H.; Wang, L.-S. *J. Chem. Phys.* **1997**, *107*, 16.
(75) Ramond, T. M.; Davico, G. E.; Hellberg, F.; Svedberg, F.; Salén, P.; Söderqvist, P.; Lineberger, W. C. *J. Mol. Spectrosc.* **2002**, *216*, 1.
(76) Blomberg, M. R. A.; Siegbahn, P. E. M.; Strich, A. *Chem. Phys.* **1985**, *97*, 287.
(77) Bauschlicher, C. W., Jr. *J. Phys. Chem. A* **2004**, *108*, 2871.
(78) Song, J.; Aprá, E.; Khait, Y. G.; Hoffmann, M. R.; Kowalski, K. *Chem. Phys. Lett.* **2006**, *428*, 277.
(79) Gutsev, G. L.; Rao, B. K.; Jena, P. *J. Phys. Chem. A* **2000**, *104*, 11961.
(80) Pierloot, K. *Mol. Phys.* **2003**, *101*, 2083.
(81) Deng, K.; Yang, J.; Zhu, Q. *J. Chem. Phys.* **2003**, *118*, 6868.
(82) Vancoillie, S.; Pierloot, K. *J. Phys. Chem. A* **2008**, *112*, 4011.
(83) Sauri, V.; Serrano-Andrés, L.; Shahi, A. R. M.; Gagliardi, L.; Vancoillie, S.; Pierloot, K. *J. Chem. Theory Comput.* **2011**, *7*, 153.
(84) Vancoillie, S.; Malmqvist, P.-Å.; Pierloot, K. *ChemPhysChem* **2007**, *8*, 1803.
(85) Chow, C.; Chang, K.; Willett, R. D. *J. Chem. Phys.* **1973**, *59*, 2629.
(86) Szilagyi, R. K.; Metz, M.; Solomon, E. I. *J. Phys. Chem. A* **2002**, *106*, 2994.
(87) Lias, S. G.; Bartmess, J. E.; Liebman, J. F.; Holmes, J. L.; Levin, R. D.; Mallard, W. G. *J. Phys. Chem. Ref. Data* **1988**, *17*, 1.

DOI: 10.1021/acs.jctc.5b00191
J. Chem. Theory Comput. 2015, 11, 3010−3021